Geological Survey of Finland, Special Paper 51

Outokumpu Deep Drilling Project 2003–2010

Edited by
Ilmo T. Kukkonen

Geological Survey of Finland
Espoo 2011

Online version of this publication can be downloaded at http://arkisto.gtk.fi/sp/sp51/sp51.pdf.
Unless otherwise indicated, the figures have been prepared by the authors of the article.

ISBN 978-952-217-151-1 (hardcover)
ISBN 978-952-217-152-8 (PDF)
ISSN 0782-8535

Layout: Elvi Turtiainen Oy
Printing house: Vammalan Kirjapaino Oy

Outokumpu Deep Drilling Project 2003–2010
Edited by Ilmo T. Kukkonen
Geological Survey of Finland, Special Paper 51, 207–218, 2011

CHARACTERISTICS OF ELASTIC PROPERTIES OF THE CRYSTALLINE ROCK SAMPLES FROM THE OUTOKUMPU DEEP DRILL HOLE: RESULTS OF ACOUSTOPOLARISCOPIC LABORATORY MEASUREMENTS

by
Felix F. Gorbatsevich, Mikhail V. Kovalevsky and Olga M. Trishina*

Gorbatsevich, F. F., Kovalevsky, M. V. & Trishina, O. M. 2011. Characteristics of elastic properties of the crystalline rock samples from the Outokumpu Deep Drill Hole: results of acoustopolariscopic laboratory measurements. *Geological Survey of Finland, Special Paper 51*, 207–218, 5 figures and 1 table.

We present the results of laboratory measurements of the elastic and nonelastic properties of drill core samples from depths of 94–2298 m in the Outokumpu Deep Drill Hole, eastern Finland. A total of 43 cubic rock samples were prepared (30–40 mm side length) and measured with the method of acoustopolariscopy under ambient conditions. In addition, the average velocities were calculated from the modal composition of the rocks. The measurement results provide the complete velocity matrices of the samples with the main components of P-waves as well as S-waves and their anisotropy factors. From the surface down to a depth of ~1300 m (mostly metasediments), the Outokumpu rocks were found to be strongly anisotropic. The lowest measured anisotropy values were observed in the ~1300–1600 m depth range (ophiolite-derived altered ultramafic rocks and metasediments). In the lower part of the hole from 1600 m to the hole bottom (metasediments and pegmatitic granite), the velocity anisotropy was variable. The effect of linear acoustic anisotropic absorption (LAAA) is exhibited in samples from the upper and lower sections of the drill hole. We attribute the variations in P- and S-wave velocities and their anisotropies to the variation in rock types and the drilling-induced relaxation of pressure (and to a minor degree temperature), which has resulted in decompaction and the formation of micro-cracks in the drill core. Therefore, a linear decrease in seismic velocities as a function of depth is observed in the laboratory measurements.

Keywords (GeoRef Thesaurus, AGI): deep drilling, cores, metamorphic rocks, igneous rocks, elastic properties, acoustopolariscopy, seismic waves, velocity, anisotropy, Outokumpu, Finland

Geological Institute of the Kola Science Centre RAS, Apatity, Russia

* *E–mail: gorich@geoksc.apatity.ru*

INTRODUCTION

The drilling of deep and superdeep drill holes requires great expenditures and they cannot therefore be widely applied for research purposes. The Outokumpu Deep Drilling Project (Kukkonen et al. 2007, 2009) aimed at the multidisciplinary exploitation of the drill core and down-hole measurements has provided an opportunity to carry out many different studies on physical and geological properties of rocks.

The Outokumpu Deep Drill Hole (R2500) was drilled in 2004–2005 by the Geological Survey of Finland using the company NEDRA as the drilling contractor. The hole reached the final depth of 2516 m in January 2005. It is located in eastern Finland about 2.5 km SE of the town of Outokumpu and the worked-out Outokumpu massive sulphide Cu-Co-Zn deposit. The drill site is located in a formation of Palaeoproterozoic metasediments (mica gneiss/schist) that hosts ophiolite-derived ultramafic rocks (serpentinite, skarn rocks) and graphitic and sulphidic schists (black schist) (Huhma 1971, 1975). The Archaean basement complex outcrops at a distance of about 20–50 km to the N and E from the Outokumpu area. A seismic reflection section was acquired before drilling and its interpretation suggested that the Outokumpu hole would mainly intersect metasediments (mica schist and black schist) and would probably meet the Archaean basement at the depth of 1.5–2 km. The main target of the drill hole was a strong, laminated seismic reflector at about 1.5 km depth (Kukkonen et al. 2007).

The final drilled section revealed that the upper part of the Outokumpu hole down to some 1310 m consists of mica schist with rare interlayers of biotite gneiss (Kukkonen et al. 2009). The 1310–1515 m interval is composed of alternating beds of black schist, biotite gneiss, serpentinite and diopside-tremolite skarn. Below 1515 m, mica schist with rare beds of black schist and quartz veins occur. From the depth of 1655 m downwards, mica schist mainly alternates with bodies of pegmatite granite and biotite gneiss. Pegmatitic granite, garnet-biotite gneiss and biotite–sillimanite schist compose the lower part of the drilled section down at 2000–2516 m. The Archaean basement was not met within the drill hole.

In the present study we report the results of measurements of elastic and nonelastic properties of drill core samples from depths of 94–2298 m in the Outokumpu drill hole using the method of acoustopolariscopy (Gorbatsevich 1999). In addition, we compare the laboratory measurements with calculated average velocities determined from the modal compositions of the samples.

Sampling and sample preparation

A total of 43 drill core samples from the Outokumpu Deep Drill Hole were received from the Geological Survey of Finland in 2006. The sample depths range from 94.0 m to 2297.85 m. First, we determined the rock types, textures, structures and compositions of the samples. A petrographic description of the rocks was prepared using thin sections. Cubic samples with a 30–40 mm edge length were cut and polished from every sample to determine seismic velocities, their anisotropies and rock densities. The cubic samples were oriented in such a way that the normal to side 3 coincided with the drill hole axis (Figure 1). The density of the samples was determined by the Archimedean principle by weighing them in air and water. Subsequently, we performed acoustopolariscopy and determined the seismic P- and S-wave velocities, the velocity matrices and the anisotropy factors of the samples. The acoustopolariscopy measurements were carried out at room temperature and pressure using non-saturated samples.

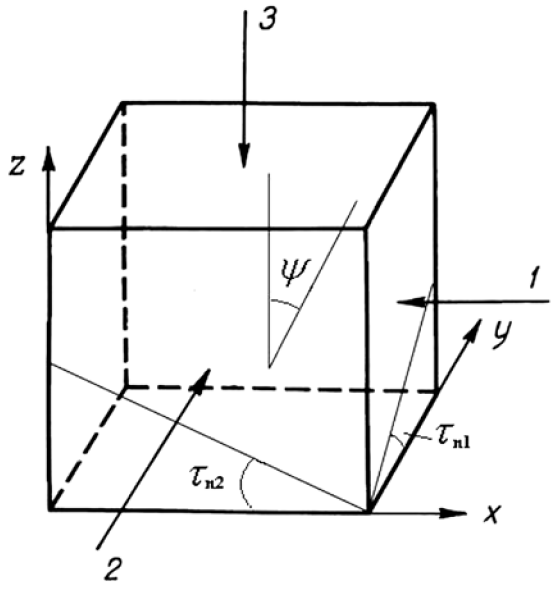

Figure 1. The shape and indexation of the samples. τ_{n1}, τ_{n2} are the angles of the symmetry elements projected to the sample sides.

METHOD AND MEASUREMENTS

The acoustopolarization method is aimed at the study of elastic and nonelastic properties of mainly anisotropic solid media (Gorbatsevich 1999, 2009). It allows the determination the presence of elastic anisotropy, the number and spatial orientation of symmetry elements, as well as the symmetry type and elasticity constants. The method is well suited to media with transverse-isotropic, rhombic and other symmetry types. The basic pattern of observations applied in this method is similar to that applied in polarization observations in optics (Volkova 1974). Acoustopolarization measurements are carried out with a specially designed device, called the acoustopolariscope (Gorbatsevich 1987). Observations are made with transducers that are able to radiate and receive purely shear linear-polarized waves.

In the first stage, measurements are made with the polarization planes of transducers parallel to each other (VP position). A sample is placed between the transducers and fixed on the rotating platform. In a sequence of measurements, the rotating platform is rotated through 360°, and signal amplitudes are measured on the screen of a recording device. In the second stage, measurements are carried out with the polarization planes of the source and receiver orthogonal to each other (90°, VC position). Again, the measurements are conducted through a 360° rotation of the sample. As a result of these measurements, we obtain acoustopolarigrams of anisotropic samples for parallel (VP) and orthogonal (VC) directions of transducer polarization.

The acoustopolarigrams measured in the VP position allow one to determine the availability of linear acoustic anisotropic absorption (LAAA) and other polarization effects (Gorbatsevich 2009). The medium in which LAAA is observed acts on the propagating beam of shear waves as a polarizer. Moreover, the directions of the 'largest' and 'smallest' amplitudes of the beam passing through the medium are related, as a rule, to the linear or planar elements, which are oriented along one common direction, such as crystalline grain borders, aligned microcracks or others (Gorbatsevich 2009). The degree of the observed LAAA is calculated according to the equation:

$$D = \frac{A_{ld} - A_{sd}}{A_{ld} + A_{sd}}, \qquad (1)$$

where A_{ld} is the size of the largest diameter of the envelopes of amplitude U_{vp} (VP position), A_{sd} is the size of diameter of the envelopes U_{vp} in the perpendicular direction to the largest diameter. According to equation (1), the medium with a full effect of LAAA has $D = 1$ (a full polarizer), and with the absence of LAAA, $D = 0$.

The effect of LAAA is present in media containing planar or linear elements. Another effect observed in seismic wave propagation through a geological medium is associated with a change in the degree of polarization of shear waves during their travel through the sample. Such a change is accompanied by an increase in the ellipticity of shear waves or by their depolarization. The shear wave depolarization (SWD) effect can be observed when shear waves propagate in a medium consisting, for instance, of differently oriented elastic anisotropic layers (Gorbatsevich 2009). The SWD effect is also rather frequently observed in anisotropic crystalline rocks composed of grains whose elastic symmetry is sufficiently maintained in two directions.

Longitudinal (P-wave) and shear velocity (S-wave) values in directions of elastic symmetry elements can be determined with the acoustopolarigrams, measured in the VC position. Velocity values are recorded according to the q-matrix ('quasi-matrix') V_{ij} (Gorbatsevich 2009):

$$\begin{matrix} V_{11} & V_{12} & V_{13} \\ V_{21} & V_{22} & V_{23} \\ V_{31} & V_{32} & V_{33} \end{matrix}, \qquad (2)$$

where V_{11} is the longitudinal wave velocity propagating in the direction along the normal to the first pair of the sample cube sides; V_{22} and V_{33} accordingly to the second and third pairs of the cube sides; V_{12} is the shear wave velocity in the direction along the normal to the first pair of the cube and the polarization vector directed normally to the second pair of the cube sides; V_{13} is also a shear wave velocity measured in the same direction but the vector of polarization is directed normally to the third pair of the cube sides. The values of V_{21} and V_{23} are measured in the direction to the second pair of the cube sides, with the vector of polarization directed to the first and third sides accordingly. The same principle refers to the values V_{31} and V_{32}.

The values of q-matrix V_{ij} components are used for the calculation of anisotropy factors A_P and B_S. The factor A_P is calculated using the velocities V_{11}, V_{22} and V_{33}:

$$A_P = \frac{1}{V_{av}}\sqrt{(V_{11}-V_{av})^2+(V_{22}-V_{av})^2+(V_{33}-V_{av})^2}, \quad (3)$$

$$V_{av} = (V_{11} + V_{22} + V_{33})/3, \quad (4)$$

where V_{av} is the average velocity of P-waves in an anisotropic sample. The value of V_{av} may be considered to be equivalent to the q-matrix spherical tensor.

The factor of anisotropy B_S (the birefringence factor) is calculated for each pair of cube sides. For example, the birefringence factor for side 1 is equal to (Clark et al. 1983):

$$B_1 = \frac{2(V_{12}-V_{13})}{V_{12}+V_{13}}. \quad (5)$$

Factors B_2 and B_3 for sides 2 and 3 are calculated using V_{21}, V_{23}, V_{31} and V_{32}. A general index of the sample anisotropy is obtained as the geometric mean of anisotropy factors for every side:

$$B_S = \sqrt{(B_1 + B_2 + B_3)}. \quad (6)$$

Using eq. 6 one may introduce a characteristic parameter that reflects the anisotropy degree of the sample as a whole.

Practical applications of the acoustopolarization method in investigations of elastic-anisotropic properties of the core from the Kola Superdeep borehole (SG-3) revealed a correlation between the obtained anisotropy data and the anisotropy parameters determined under *in situ* conditions (Orlov & Laverov 1998, Golovataya et al. 2006). For instance, when loading anisotropic samples, the spatial orientation of the symmetry elements does not change (Lokajíček et al. 2000). The anisotropy characteristics obtained with acoustopolariscopy also show a correlation with the SG-3 technical parameters (Orlov & Laverov 1998, Gorbatsevich 2009). In the 2.5-km-deep Outokumpu hole, the pressure and temperature range is not very wide (<67 MPa and <40°C; Kukkonen et al. 2007), but the pressure difference between surface and hole bottom is expected to generate a difference of about 10–20% between velocities measured in the laboratory at room P and T and those prevailing *in situ* at the hole bottom. The acoustopolarization method provides interesting data on elastic properties of the Outokumpu R2500 core samples. A proportional relationship is expected between the velocity and anisotropy data obtained at room temperature and pressure and those obtained in the simulated *in situ* conditions (Golovataya et al. 2006).

RESULTS

A complete listing of the results of laboratory measurements is provided in Table 1. The results from eight samples representative of typical rocks of the drill hole section are displayed in Figures 2 (thin-section photographs) and 3 (acoustopolarigrams), and discussed in more detail below: ODB-153_20 (garnet-biotite schist with graphite), ODB-599_00 (garnet-biotite schist with graphite), ODB-1101_30 (biotite-muscovite schist with veinlets of gypsum-carbonaceous composition), ODB-1414_75 (serpentinite), ODB-1488_65 (diopside-tremolite rock), ODB-1893_80 (mica-plagioclase coarse-grained granite with garnet), ODB-2155_15 (mica pegmatite with garnet), ODB-2297_25 (biotite schist). Table 1 presents the petrographic properties of the 43 samples: values of rock density ρ, the matrix of velocities V_{ij}, anisotropy factors A_P and B_S, calculated indexes of linear acoustic anisotropic absorption D, and the angles τ_{n1}, τ_{n2} of the symmetry elements of projections with reference to the sample sides.

Figure 4 illustrates the depth dependencies of longitudinal (V_P) and shear (V_S) wave velocities in the Outokumpu section: V_P(e) and V_S(e) are the experimentally measured values of the samples calculated as averages using V_{ij} matrixes presented in Table 1; V_P(p) and V_S(p) were calculated from the mineral (modal) composition of rocks using the method of Belikov et al. (1970).

The calculated V_P(p) and V_S(p) values for mica schist and the pegmatitic granite do not seem to show any systematic depth dependence, which we attribute to the homogeneous composition of the rock types, and relatively similar velocity values. However, higher variation of V_P(p) and V_S(p) is observed at 1.3–1.5 km, where the ophiolite-derived serpentinite and skarn rock layers alternate. The average calculated velocities are V_P(p) = 5.8 km/s and V_S(p) = 3.6 km/s.

On the other hand, the experimental V_P(e) and

Table 1. Elastic and nonelastic properties of rock samples along the Outokumpu drill hole section.

Number of sample	Name of rock	Depth of excavation H, m	Density ρ, g/cm^3	Matrix of velocities V_{ij}, km/s	Anisotropy factors		LAA factor D_1, D_2, D_3	Angle of symmetry element projections	
					A_P	B_S		τ_{n1} degrees	τ_{n2} degrees
ODB-94_00	Sill-Bi schist	94.00	2.74	5.04 3.25 2.51 3.19 4.70 2.46 2.59 2.66 3.38	0.284	0.364	0.22 0.64 0.65	60 19 30	165 128 111
ODB-153_20	Grt-Bt schist with Gr	153.2	2.74	5.45 3.62 2.96 3.61 6.00 2.97 2.88 2.96 4.55	0.194	0.281	0.22 0.24 0.13	16 80 -	104 172 -
ODB-202_20	Bt-schist with graphite	202.2	2.74	5.95 3.72 3.24 3.74 6.37 3.42 3.26 3.16 5.51	0.102	0.167	0.22 0.13 0.09	7 67 46.5	93 168 147
ODB-247_45	Bt- schist with graphite	247.45	2.74	5.96 3.76 3.30 3.73 6.35 3.32 3.37 3.34 5.41	0.113	0.175	0.05 0.06 0.05	81 56 84	170 138 167
ODB-319_25	Grt-Bi schist with graphite	319.25	2.74	6.26 3.78 3.41 3.60 5.95 3.39 3.35 3.29 5.23	0.129	0.121	0.04 0.12 0.07	65 59 67	156 152 134
ODB-351_90	Grt-Bt-Chl schist with graphite	351.9	2.77	6.29 3.82 3.99 3.63 5.85 3.69 3.48 3.29 4.86	0.182	0.073	0.07 0.11 0.5	15 87 7	103 176 97
ODB-391_70	Bt- schist with graphite	391.7	2.73	5.45 3.47 3.11 3.69 6.06 3.25 3.22 3.28 5.00	0.137	0.169	0.08 0.05 0.08	61 24 86	152 116 171
ODB-450_55	Biotite gneiss	450.55	2.81	5.47 3.64 3.69 3.70 6.34 2.68 2.82 2.90 4.15	0.293	0.321	0.45 0.09 0.26	21 24 25	115 110 115
ODB-506_10	Bt- schist with graphite	506.1	2.74	6.34 3.77 3.08 3.72 6.02 3.12 3.19 3.17 5.44	0.109	0.267	0.2 0.15 0.06	80 10 90	171 108 177
ODB-599_00	Grt-Bi schist with graphite	599	2.74	5.72 3.60 3.39 3.58 6.16 3.44 3.38 3.42 5.47	0.085	0.077	0.05 0.01 0.05	88 3 15	177 95 115
ODB-703_25	Grt-Bi schist with graphite	703.25	2.75	6.18 3.80 3.10 3.58 5.59 3.07 3.08 3.15 4.89	0.164	0.255	0.14 0.16 0.12	16 4 40	102 99 112
ODB-801_40	Grt-Bi schist with graphite	801.4	2.78	5.86 3.48 3.65 3.52 5.41 3.16 3.44 2.56 5.09	0.101	0.316	0.08 0.13 0.28	23 6 90	117 104 165
ODB-900_25	Grt-Bi schist with graphite	900.25	2.74	5.05 3.51 2.39 3.48 5.54 2.44 2.82 2.46 2.53	0.522	0.535	0.22 0.09 0.46	89 75 35	174 171 105
ODB-1000_50	Bt- schist with graphite	1000.5	2.73	6.15 3.71 3.12 3.67 5.56 3.14 3.11 3.18 4.27	0.255	0.234	0.1 0.22 0.07	8 82 82	97 168 164
ODB-1101_30	Bt-Ms schist with veinlets of gypsum-carbonaceous composition	1101.3	2.76	4.45 3.26 3.22 3.22 5.44 2.50 2.02 2.43 2.85	0.435	0.312	0.9 0.81 0.51	10 8 110	104 106 177
ODB-1202_40	Grt-Bi schist with graphite	1202.4	2.71	4.85 3.32 2.92 3.39 5.92 3.21 3.06 3.24 4.44	0.213	0.151	0.21 0.02 0.11	82 18 8	162 114 94
ODB-1300_70	Ore Bt- schist with graphite	1300.7	2.75	5.88 3.47 2.82 3.43 5.58 2.81 2.84 2.92 4.48	0.196	0.288	0.18 0.11 0.02	11 15 64	98 105 149
ODB-1317_75	Ore black schist	1317.75	2.85	6.06 3.45 3.39 3.50 5.53 3.52 3.31 3.36 5.27	0.101	0.024	0.09 0.11 0.05	19 6 2	115 102 90
ODB-1327_80	Ore Di-Trem rock with carbonate	1327.8	3.22	6.66 3.80 3.90 3.88 6.51 3.95 3.93 3.97 6.31	0.038	0.033	0.11 0.09 0.48	12 6 85	106 101 176

Table 1. (cont.)

Number of sample	Name of rock	Depth of excavation H, m	Density ρ, g/cm^3	Matrix of velocities V_{ij}, km/s	Anisotropy factors		LAA factor D_1, D_2, D_3	Angle of symmetry element projections	
					A_P	B_S		τ_{n1} degrees	τ_{n2} degrees
ODB-1394_60	Serp-Trem rock with ore mineral	1394.6	2.80	6.42 3.64 3.68 3.70 6.70 3.50 3.36 3.42 6.20	0.055	0.059	0.03 0.04 0.01	79 37 5	162 124 93
ODB-1414_75	Serpentinite	1414.75	2.49	4.21 2.28 2.18 2.27 4.27 2.13 2.16 2.18 4.11	0.027	0.078	0.21 ~0.7 0.04	75 70 62	160 162 161
ODB-1416_95	Serpentinite with more c/g veinlets of Serp	1416.95	2.51	4.02 2.39 2.17 2.32 4.36 2.27 2.24 2.26 4.08	0.062	0.099	0.68 0.15 0.45	22 30 0	100 120 90
ODB-1427_85	Serpentinite with Trem	1427.85	2.69	5.75 3.14 3.06 2.97 5.99 3.17 2.90 2.89 5.68	0.04	0.068	0.04 0.4 0.02	38 64 54	125 156 160
ODB-1458_00	Serpentinite	1458	2.63	5.55 2.81 2.56 2.88 5.46 2.85 2.64 2.61 5.27	0.037	0.094	0.09 0.1 0.09	10 23 52	113 114 138
ODB-1465_40	Serpentinite with talk veinlets	1465.4	2.54	4.73 2.43 2.38 2.41 4.66 2.57 2.34 2.48 4.72	0.012	0.089	0.19 0.51 0.26	19 16 60	106 111 157
ODB-1473_60	Serpentinite	1473.6	2.52	4.42 2.49 2.48 2.58 4.21 2.03 2.12 2.06 1.61	0.649	0.238	0.42 0.82 0.57	23 13 22	96 125 120
ODB-1488_65	Di-Trem rock	1488.65	3.26	4.85 3.19 2.94 3.14 5.38 2.95 3.06 3.10 4.79	0.092	0.104	0.11 0.21 0.23	72 50 19	162 176 128
ODB-1513_88	Black schist with ore mineral veinlets	1513.88	2.88	5.58 3.30 3.45 3.40 5.55 3.36 3.46 3.26 5.58	0.004	0.075	0.21 0.14 0.07	50 68 60	139 143 152
ODB-1664_80	Pegmatophyre with Ms	1664.8	2.66	5.00 3.40 3.24 3.14 5.16 3.16 3.14 3.08 4.58	0.086	0.052	0.08 0.42 0.03	48 31 41	136 150 151
ODB-1700_85	Bt- schist	1700.85	2.74	5.22 2.71 2.52 2.72 4.82 2.64 2.58 2.44 3.20	0.343	0.096	0.31 0.78 0.36	0 17 32	90 114 127
ODB-1724_75	Ore black schist	1724.75	2.84	5.32 3.30 3.05 3.26 5.22 3.04 3.15 2.87 4.64	0.103	0.143	0.08 0.11 0.05	60 78 42	148 166 139
ODB-1751_05	Grt-Bt schist	1751.05	2.77	4.08 2.63 2.21 2.52 3.93 2.17 2.25 2.16 2.33	0.398	0.233	0.1 0.29 0.76	55 36 62	163 117 136
ODB-1803_80	Bt- schist	1803.8	2.75	4.04 2.83 2.89 2.84 4.59 2.76 2.64 2.72 3.56	0.179	0.046	0.21 0.14 0.36	84 78	163 173
ODB-1850_85	Bt- schist	1850.85	2.77	4.61 3.21 2.33 3.16 5.17 2.39 2.24 2.35 2.99	0.376	0.425	0.08 0.08 0.29	24 22 34	105 107 114
ODB-1893_80	Mc-Pl. Grt- containing coarse granite	1893.8	2.65	5.09 3.01 3.18 3.02 5.05 3.16 3.16 3.08 4.65	0.07	0.051	0.02 0.71 0.25	13 33 75	114 127 138
ODB-1940_00	Bt-Sill schist	1940.00	2.79	4.77 3.12 2.05 3.05 4.45 2.05 2.08 1.97 2.33	0.487	0.573	0.1 0.53 0.08	69 55 13	170 144 103
ODB-1995_00	Bt-schist	1995.00	2.78	4.82 2.92 2.93 3.05 4.26 2.01 1.98 1.94 2.33	0.486	0.412	0.68 0.93 0.41	10 14 75	100 100 154
ODB-2041_30	Ms-Sill pegmatophyre	2041.3	2.64	4.73 3.08 3.12 2.99 5.13 3.00 2.92 3.05 4.83	0.061	0.046	0.06 0.01 0.4	7 57 8	105 156 117

Table 1. (end)

Number of sample	Name of rock	Depth of excavation H, m	Density ρ, g/cm^3	Matrix of velocities V_{ij}, km/s	Anisotropy factors		LAA factor D_1, D_2, D_3	Angle of symmetry element projections	
					A_P	B_S		τ_{n1} degrees	τ_{n2} degrees
ODB-2105_20	Two-mica pegmatophyre	2105.2	2.60	3.02 2.46 2.73 2.39 4.27 2.38 2.43 2.43 5.06	0.353	0.104	0.35 0.47 0.47	10 40 30	94 158 137
ODB-2155_15	Mc- pegmatite with Grt	2155.15	2.62	4.62 2.88 2.90 2.89 4.53 2.67 2.92 2.89 4.95	0.067	0.08	0.1 0.09 0.66	- - 29	- - 121
ODB-2199_80	Pegmatophyre with Grt	2199.8	2.65	3.78 2.58 2.63 2.67 4.04 2.59 2.70 2.60 3.99	0.049	0.052	0.07 0.08 0.35	46 9 47	139 115 125
ODB-2253_00	Grt-Bt schist	2253.00	2.73	4.49 2.78 2.29 3.00 4.28 2.91 2.38 2.35 2.35	0.451	0.196	0.03 0.46 0.72	17 14 13	112 102 116
ODB-2297_85	Bt-schist	2297.85	2.72	4.65 2.99 2.20 2.97 4.72 2.19 2.31 2.32 3.34	0.259	0.429	0.38 1.00 0.06	94 16 59	174 77 116

[1] Mineral abbreviations according to Kretz (1983).

V_S(e) values show a general tendency of decreasing values with increasing depth. These trends are approximately linear (Figure 4). The observed trends of V_P(e) and V_S(e) with depth are very likely due to drilling-related decompaction and stress-relaxation effects and the subsequent formation of microfractures in the drill core. Small air-filled volumes of microfractures easily reduce the velocities. A similar effect has previously been reported from the samples of the Kola superdeep borehole SG-3 (Gorbatsevich 2003).

The most dramatic variation in the V_P(e) and V_S(e) values is observed in the ~1300–1550 m depth range, which is attributed to the variation in the mineral composition of the rocks. The results are in line with the velocities calculated from mineral composition V_P(p) and V_S(p), but only showing lower values because of the micro-fractures. The conclusion on the effect of rock type variation is also supported by the measured rock densities (Figure 5).

According to the acoustopolarization measurements, rocks from the upper section mainly comprising metasediments are very homogeneous (down to a depth of about 1300 m) and highly anisotropic. Samples with the orthorhombic symmetry type prevail. Acoustopolarigrams of the samples ODB-153_20, ODB-599_00, and ODB-1101_30 corroborate the above conclusion (Figure 3). Judging from the acoustopolarigrams, the samples are characterized by marked homogeneity of elastic-anisotropic properties. In a certain sense, the rock symmetry within this part of the drill hole section can be envisaged to be similar to the anisotropic behaviour of an orthorhombic crystal ('quasi-crystal' behaviour; Gorbatsevich 2009). The homogeneity can be explained by a well-developed planar orientation of elongated grains of minerals (Figure 2) such as biotite and plagioclase (Table 1). The development of such textures can be explained by the long-term action (in geological time scales) of the stress fields of two types: either $T_z \neq T_2 = T_3$ or $T_z \neq T_2 \neq T_3$, where T_z is the vertical component, and T_2 and T_3 are the horizontal stress components (Brace 1960, Kozhevnikov 1982, Gorbatsevich 2009).

The part of the section within 1310–1515 m is characterized by a rather complex palaeogeodynamic environment with quite different conditions of grain formation in rock minerals as compared with those in the section above. A typical example of this is the thin section of the sample ODB-1414_75 (serpentinite). The sample (Figure 2, Table 1) is mainly composed of serpentine showing a reticulate structure. The relict porphyroid texture of the rock is due to the presence of coarse grains of olivine fully substituted by serpentine, and the olivine grains separated by a fine-grained ground mass composed of serpentine and ore minerals. The acoustopolarigrams (Figure 3) reflect the complicated rock texture. For instance, in the thin section one can single out the elements that form some trigonal symmetry (Figure 2). This rock can be considered to be weakly anisotropic, heterogeneous and displaying the LAAA effect (on the sample face 2).

Another sample of diopside-tremolite rock, ODB-1488_65 from the 1330–1510 m range,

shows considerable heterogeneity in structure both in the thin section and on the acoustopolarigrams (Figures 2 and 3). In the thin section one can see a reticulate, porphyroid and streaky texture. The mineral grains have isometrical elongated shapes and differ greatly in size. Accordingly, the acoustopolarigrams of all three pairs of faces (Figure 3) reflect heterogeneity of the structure, and chaotic spatial orientation of the elastic symmetry elements in the mineral grains. On the first and especially second faces of the sample, the effect of SWD is present. In this case, it is caused by a different orientation of the symmetry elements in the neighbouring grains.

The acoustopolarigrams of the lower part (1515–2516 m) of the OKU section (see the examples of ODB-1893_80, ODB-2155_15 and ODB-2297_85 in Figure 3) show that their structures are more ordered than that of the preceding samples, but they are also heterogeneous. They demonstrate the presence of the LAAA effect, which can be explained by the availability of plagioclase and mica. On the whole, the rock of these samples may be characterized as heterogeneous and aniso-

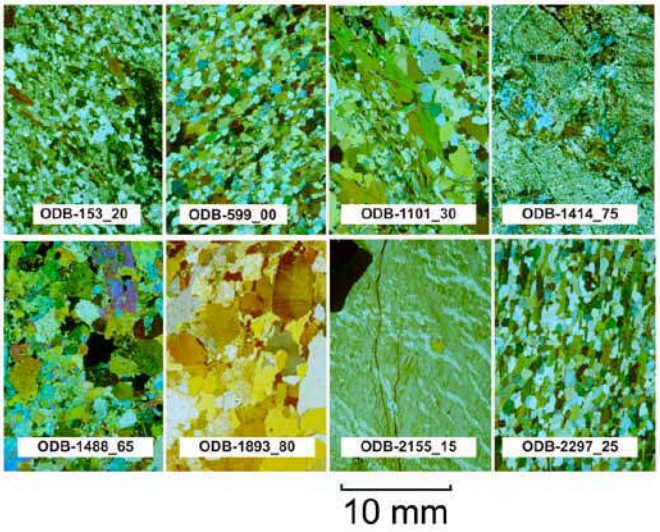

Figure 2. Thin-section photographs of drill core samples from the Outokumpu Deep Drill Hole. From left to right, top: ODB-153_20 (garnet-biotite schist with graphite), ODB-599_00 (garnet-biotite schist with graphite), ODB-1101_30 (biotite-muscovite schist with veinlets of gypsum-carbonaceous composition), ODB-1414_75 (serpentinite); bottom: ODB-1488_65 (diopside-tremolite rock), ODB-1893_80 (mica-plagiclase coarse-grained garnet containing granite), ODB-2155_15 (mica pegmatite with garnet), ODB-2297_25 (biotite schist).

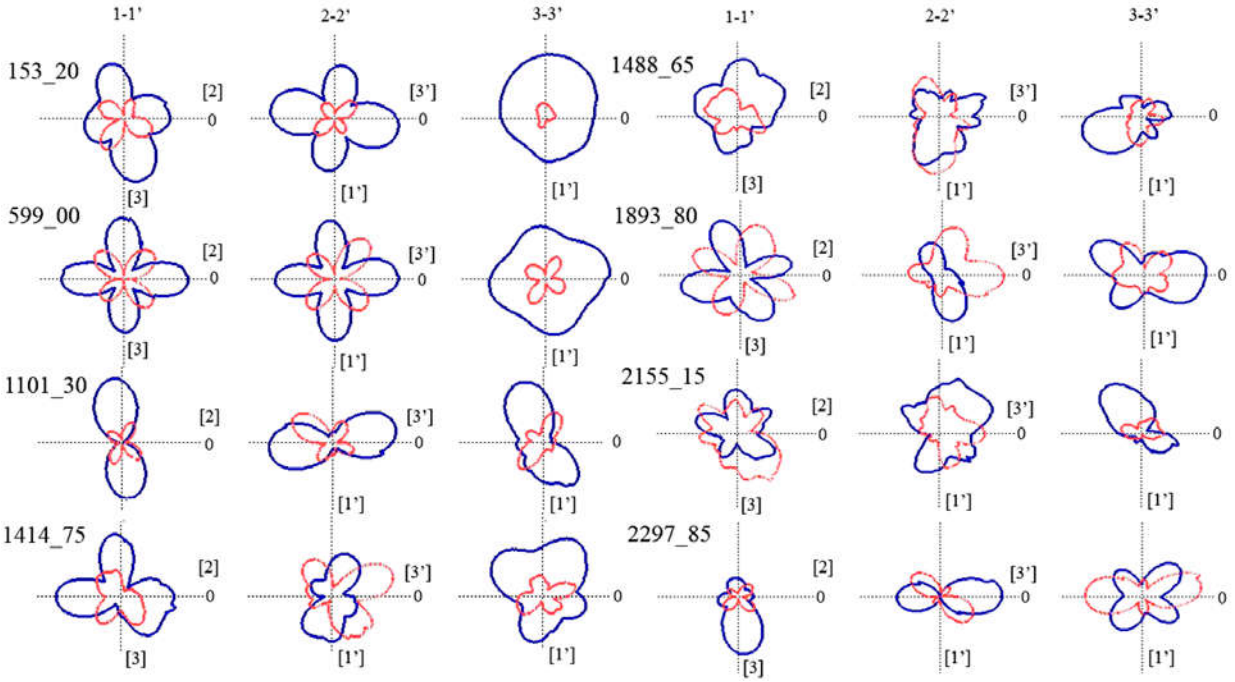

Figure 3. Acoustopolarigrams of the rock samples ODB-153_20, ODB-599_00, ODB-1101_30, ODB-1414_75, ODB-1488_65, ODB-1893_80, ODB-2155_15, ODB-2297_25 from the Outokumpu Deep Drill Hole. Diagrams labelled 3-3' refer to the plane perpendicular to the vertical Z axis, and 1-1' and 2-2' to planes perpendicular to the horizontal X and Y axis. The blue line is for acoustopolarigrams measured in the VP position (transducer polarization planes parallel), and the red line for acoustopolarigrams in the VC position (transducer polarization planes orthogonal). For rock types of the samples, see the legend of Figure 2.

tropic with a manifestation of LAAA. This can be explained by the coarse crystalline texture of rocks and their pegmatoid fabric (Figure 2, Table 1). For instance, the sample ODB-2155_15 (pegmatite) has a porphyroid structure and is composed of large microcline-perthite crystals. When the rock texture is more homogeneous, its acoustopolarigrams have a more orderly shape (Figure 3, sample ODB-2297_85 of biotite schist). On the whole, the acoustopolarigrams presented in Figure 3 are typical of all samples from the lower section of the Outokumpu hole. LAAA and SWD effects were registered in them to varying degrees. The manifestation of similar effects was first discovered in the samples from the Kola superdeep borehole (Orlov & Laverov 1998).

The variations in anisotropy parameters as a function of depth, determined using P-waves

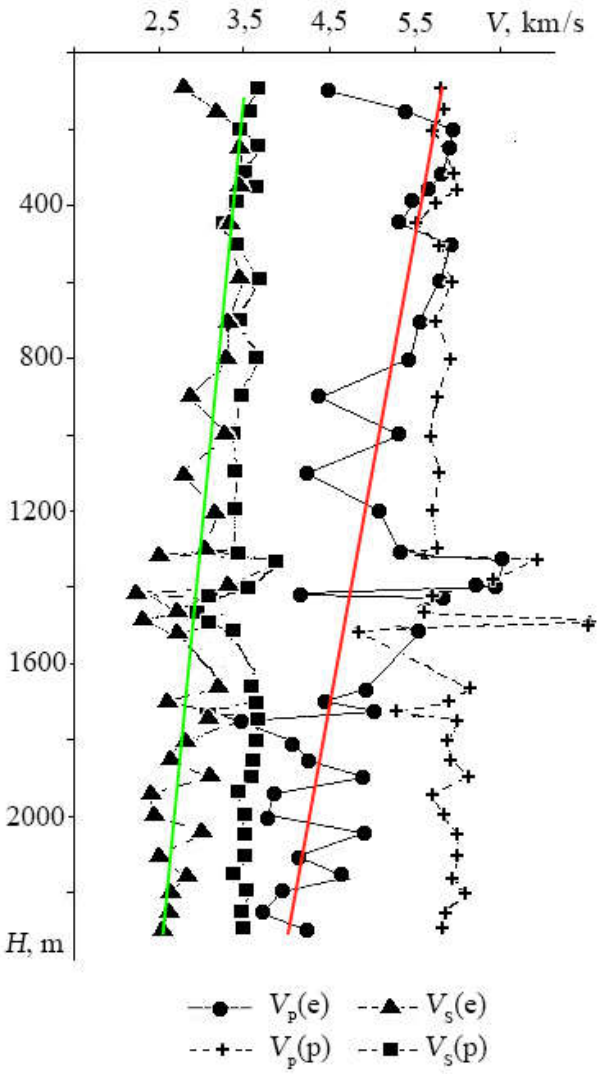

Figure 4. Depth dependencies of P-wave (V_P) and S-wave (V_S) velocities in the Outokumpu Deep Drill Hole section. V_P(e) and V_S(e) were experimentally measured from the samples using acoustopolariscopy, whereas V_P(p) and V_S(p) were calculated based on the mineral composition of the rocks.

(A_P) and S-waves (B_S) (Table 1 and Figure 5), are more or less identical. From the surface down to a depth of ~800 m, A_P and B_S are between 0.1 and 0.3. In the 800–1100 m depth range their values attain values between 0.2–0.5. The lowest values of anisotropy are observed in the ~1300–1600 m range (<0.1). Beneath 1600 m down to the drill hole bottom, A_P and B_S increase again but show a wide range of values (0.1–0.5). The variations in A_P and B_S generally correlate with the variation of rock types in the hole. However, at deeper levels the effect of microfractures gradually increases, and starts to mask the anisotropy effects due to mineral composition and texture.

A non-hydrostatic stress field acting under metamorphic conditions (elevated pressure and/or temperature) on polymineral rocks over geological time scales will result in re-orientation of crystallographic axes and planes of minerals (Robin 1979, Kozhevnikov 1982, Gorbatsevich 2009) and result in anisotropic structures. We may suggest that a homogeneous and stable orientation of the palaeostress field acted in the <1300 m depth range. In the ~1300–1600 m depth range the palaeostresses were rather low. Below 1600 m down to the drill hole bottom, the action of palaeostresses is only manifested in phyllosilicate rocks.

A relationship between rock anisotropy and the drill hole deviation has earlier been reported from the Kola superdeep hole and other deep drill holes (Orlov & Laverov 1998, Gorbatsevich & Smirnov 2000). The relationship suggests that the hole deviation would at least partly be controlled by rock properties. Drillers traditionally know that inclined rock layers tend to turn the orientation of the hole, and the geology is certainly one factor contributing to geometries of deep holes. However, it is difficult to distinguish the effects of active engineering control of borehole deviation and pure geological factors. In the Outokumpu case, the comparison of A_P and B_S and the angle of the drill hole deviation Δ from the vertical (Figure 5) indicates no correlation. Correlation factors (R^2) are smaller than 0.01. Even though the rock anisotropy and inclined layers probably affected the hole orientation in the Kola Superdeep case, we cannot report such an observation in the Outokumpu R2500 hole. This may be due to subhorizontal dip angles of strata in Outokumpu. However, it should also be taken into account that when the drill hole was becoming increasingly deviated from vertical during drilling, the hole was decidedly forced to turn back towards vertical at depths exceeding ~1 km. This finally secured the subvertical geometry of the borehole track (I. Kukkonen, written comm. 2010).

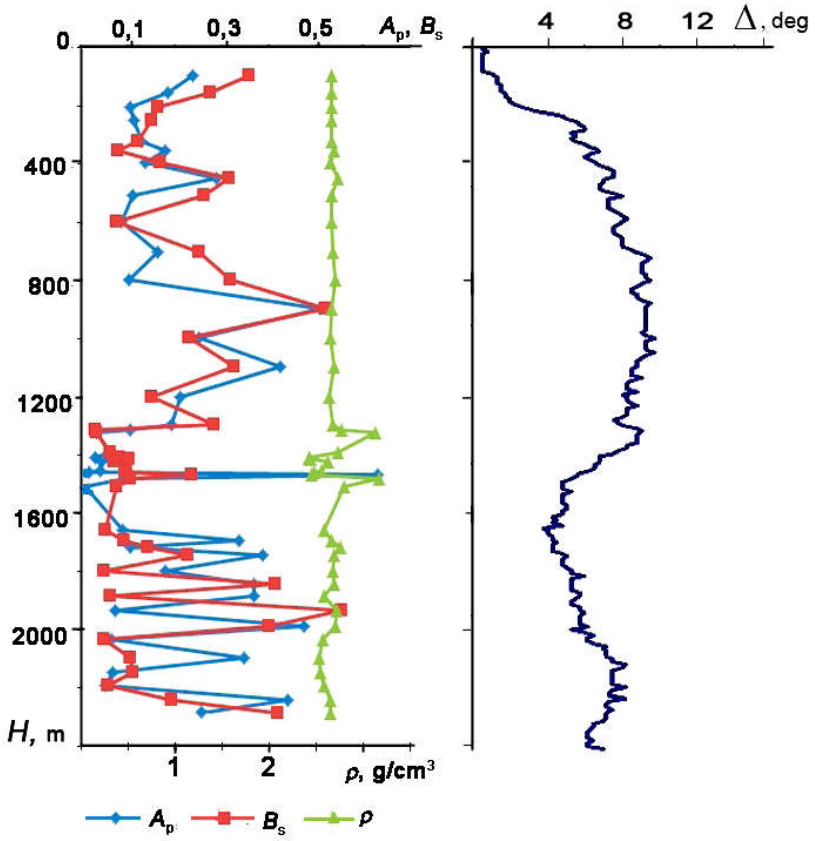

Figure 5. Depth dependencies of elastic anisotropy factors A_P and B_S, density ρ, and the angle of inclination (Δ) of the OKU from the vertical in the section of the Outokumpu Deep Drill Hole.

DISCUSSION

The acoustopolarization measurements of the samples from the upper section of the Outokumpu Deep Drill Hole (to a depth of ~1300 m) showed a high degree of anisotropic orientation of the rock texture as revealed by the acoustopolarigrams indicating a 'quasi-crystal' type of behaviour. Neutron texture measurements on fabric-related anisotropy of the Outokumpu samples also yielded a well-developed similar anisotropy for the mica schists (Ivankina et al. 2007). Ivankina et al. (2007) demonstrated that all samples from the upper part of the Outokumpu section (five samples in the depth interval 578–1093 m) show a strong orientation especially controlled by phyllosilicates (biotite and muscovite) but also contributed to by quartz and plagioclase. Such a well-developed schistose texture along with the orientation of crystallographic axes of mineral grains and oriented microfracturing is able to generate medium and high elastic anisotropy in these rocks (Kern et al. 2008).

The average calculated velocities V_P(p) and V_S(p) (Figure 4) are slightly higher than those obtained by Elbra et al. (2009) from water-saturated Outokumpu samples. These data are also close to those calculated from the rock mineral composition and measured under elevated pressure and temperature (Kern & Mengel 2009), as well as measured *in situ* by the sonic logging method (Heinonen et al. 2009). Regarding the published data, the average values of V_P are in the range of 5.6–6.0 km/s in the Outokumpu Deep Hole section. The exception is the 1310–1515 m interval, where rapid changes in rock types occur and the P-wave velocity values vary in a wide range from 4 to 7 km/s.

The pressure dependencies of V_P and the anisotropy factor of P-wave velocity, A-V_P, of the Outokumpu rocks were investigated by Kern et al. (2008) and Kern & Mengel (2009). According to these results, the P-wave anisotropy is highest in the biotite gneisses, which constitute about 70% of the 2500-m crustal section, and lowest in the serpentinites, representing major lithologies within the meta-ophiolite series. The anisotropy factors rapidly decrease as a function of increasing

pressure up to about 100 MPa before stabilizing to a linear dependence at higher pressures. This was attributed to the closing of cracks and pores with pressure. Our determinations of anisotropy based on compression and shear waves measured under ambient conditions (Figure 5) are in line with these results and indicate that the role of microfractures is relevant in influencing the elastic properties of the Outokumpu samples.

According to Table 1 and Figure 5, the rock density varies only slightly around the average ρ = 2.74 g/cm^3 in the metasediments and pegmatitic granite. On the other hand, strong density variation occurs in the 1310–1515 m interval characterized by the ophiolite-derived altered ultrabasic rocks serpentinite and skarns rocks (Figure 5; see also Kern & Mengel 2009, Heinonen et al. 2009). The previous investigations have shown that the decompaction effect influences the rock density to a much lesser degree than the velocity (Orlov & Laverov 1998, Golovataya et al. 2006). For instance, our estimation for the 2.5 km depth is that the change in the rock density under the decompaction effect will not exceed 1% (the approximate pressure at a depth of 2.5 km is $P \approx 67$ MPa, and temperature is about 40 °C (Kukkonen et al. 2009)). This estimation is based on data for compositionally similar rocks (Golovataya et al. 2006). Therefore, density variations can be attributed to variations in the mineral composition of the low-porosity crystalline rock, and variations due to pressure and temperature are negligible for density in the depth range of the Outokumpu Deep Drill Hole.

CONCLUSIONS

According to the acoustopolarization measurements, rocks in the upper section of the hole (down to a depth of about 1300 m) are strongly anisotropic but very homogeneous. Their homogeneity is explained by the constant composition with depth, and the well-developed metamorphic texture with preferred planar and linear orientation of elongated mineral grains (biotite, plagioclase, etc.). The acoustopolarigrams of the lower part (between 1300 m and 2300 m) show that the structure is less ordered and more heterogeneous. The samples from the Outokumpu Deep Drill Hole display the effects of linear acoustic anisotropic absorption (LAAA) and shear wave depolarization (SWD). The LAAA effect is manifested in the samples from the OKU upper and lower section to a variable degree.

P- and S-wave velocity values of the drill core samples experimentally determined under ambient laboratory conditions showed a decreasing trend with depth. The observed trends are very likely due to drilling-related decompaction and stress relaxation effects and the subsequent formation of microfractures in the drill core. The average calculated velocities for the entire Outokumpu Deep Drill Hole section determined using mineral composition are V_P(p) = 5.8 km/s, V_S(p) = 3.6 km/s. These values are also close to values determined by the down-hole logging.

The elastic anisotropy indices determined as functions of depth behave in a similar way for both compression and shear wave velocities. From the surface down to a depth of ~800 m, A_P and B_S are between 0.1 and 0.3. In the 800–1100 m depth range they attain values between 0.2–0.5. The lowest values of anisotropy (<0.1) are observed in the ~1300–1600 m range. Beneath 1600 m down to the drill hole bottom, A_P and B_S increase again, but show a wide range of values (0.1–0.5). The variations in (A_P) and (B_S) generally correlate with the variation in rock types in the hole. However, at deeper levels the effect of microfractures gradually increases, and starts to mask the anisotropy effects purely due to mineral composition and texture.

Although a relationship between rock anisotropy and the drill hole deviation has been previously reported from the Kola Superdeep hole and other deep drill holes, such a relationship does not seem to apply to the Outokumpu Deep Drill Hole. We attribute this to active engineering measures during drilling to keep the hole as vertical as possible.

ACKNOWLEDGEMENTS

We are grateful to Ilmo Kukkonen, Geological Survey of Finland, Espoo, for the Outokumpu Deep Hole drill core samples, accompanying materials and consultations. We also want to thank Valery Vetrin, Kola Science Centre of RAS, Apatity, for the petrographic and mineralogical rock descriptions.

The work has been performed in the framework of projects № 07-05-00100-a and 10-05-00082-a, supported by the Russian Foundation for Basic Research.

REFERENCES

Belikov, B. P., Aleksandrov, K. S. & Ryzhova, T. V. 1970. Elastic properties of rock forming minerals and rocks. Moscow: Nauka. 276 p. (in Russian)

Brace, W. F. 1960. Orientation of anisotropic minerals in a stress field. Memoires of the Geological Society of America 79 (9), 9–20.

Clark, A. V., Mignogna, R. B. & Sanford, R. J. 1983. Acoustoelastic measurement of stress and stress intensity factors around crack tips. Ultrasonics 21, 57–64.

Elbra, T., Karlqvist, R., Lassila, I., Haeggström, E. & Pesonen, L. J. 2009. Ultrasonic seismic P- and S-velocities in the Outokumpu drill core: In: Kukkonen, I. T. (ed.) Outokumpu Deep Drilling Project, Third International Workshop, Espoo, Finland, November 12–13, 2009, Programme and Abstracts. Geological Survey of Finland, unpublished report Q10.2/2009/61, 29–31.

Golovataya, O. S., Gorbatsevich F. F., Kern H. & Popp T. 2006. Properties of some rocks from the section of the Kola ultradeep borehole as a function of the P-T parameters. Izvestiya, Physics of the Solid Earth 42 (11), 865–876.

Gorbatsevich, F. F. 1987. Acoustopolariscope for measuring elasticity of solid body samples. Auth. Cert. 1281993, USSR. Bull. Inv. 1. (in Russian)

Gorbatsevich, F. F. 1999. Acoustic polarization method for determining elastic symmetry and constants of anisotropy in solid media. Ultrasonics, 37, 309–319.

Gorbatsevich, F. F. 2003. Decompaction mechanism of deep crystalline rocks under stress relief. Tectonophysics 370 (1–4), 121–128.

Gorbatsevich, F. F. 2009. Acoustopolariscopy of minerals and rocks. Saarbruecken: VDM Verlag. 144 p.

Heinonen, S., Schijins, H., Schmitt, D. R., Heikkinen, P. J. & Kukkonen, I. T. 2009. High resolution reflection seismic profiling in Outokumpu. In: Kukkonen, I. T. (ed.) Outokumpu Deep Drilling Project, Third International Workshop, Espoo, Finland, November 12–13, 2009, Programme and Abstracts. Geological Survey of Finland, unpublished report Q10.2/2009/61, 17–22.

Huhma, A. 1971. Outokumpu. Geological map of Finland 1:100 000, Pre-Quaternary Rocks, Sheet 4222. Geological Survey of Finland.

Huhma, A. 1975. Outokummun, Polvijärven ja Sivakkavaaran kartta-alueiden kallioperä. Summary: Precambrian rocks of the Outokumpu, Polvijärvi and Sivakkavaara map-sheet areas. Geological Map of Finland 1:100 000, Explanation to the Maps of Pre-Quaternary Rocks, Sheets 4222, 4224, 4311. Geological Survey of Finland. 51 p.

Ivankina, T. I., Kern, H. M. & Nikitin, A. N. 2007. Neutron texture measurements and 3D velocity calculations on strongly foliated biotite gneisses from the Outokumpu deep drill hole. In: Kukkonen, I. T. (ed.) Outokumpu Deep Drilling Project, Second International Workshop, May 21–22, 2007, Espoo, Finland. Programme and Extended Abstracts. Geological Survey of Finland, unpublished report Q10.2/2007/29, 47–51.

Kern, H., Ivankina, T. I., Nikitin, A. N., Lokajicek, T. & Pros, Z. 2008. The effect of oriented microcracks and crystallographic and shape preferred orientation on bulk elastic anisotropy of a foliated biotite gneiss from Outokumpu. Tectonophysics 457, 143–149.

Kern, H. & Mengel, K. 2009. Outokumpu scientific drill hole: comparison of experimentally determined and calculated wave velocities with sonic log data. In: Kukkonen, I. T. (ed.) Outokumpu Deep Drilling Project, Third International Workshop, Espoo, Finland, November 12–13, 2009, Programme and Abstracts. Geological Survey of Finland, unpublished report Q10.2/2009/61, 23–61.

Kozhevnikov, V. N. 1982. Formation conditions of structural and metamorphic paragenesises in Precambrian complexes. Moscow: Nauka. 184 p. (in Russian)

Kretz, R. 1983. Symbols for rock-forming minerals. American Mineralogist 68, 277–279.

Kukkonen, I. T. & the Outokumpu Deep Drilling Working Group 2007. Outokumpu deep drilling project – Introduction to Geology and Geophysics of the Deep Hole and Research Within the Project. In: Kukkonen, I. T. (ed.) Outokumpu Deep Drilling Project, Second International Workshop, May 21–22, 2007, Espoo, Finland. Programme and Extended Abstracts. Geological Survey of Finland, unpublished report Q10.2/2007/29, 11–16.

Kukkonen, I. T. & the Outokumpu Deep Drilling Working Group 2009. Outokumpu deep drilling project – Introduction to Geology and Geophysics of the Deep Hole and Research Within the Project. In: Kukkonen, I. T. (ed.) Outokumpu Deep Drilling Project, Third International Workshop, Espoo, Finland, November 12–13, 2009, Programme and Abstracts. Geological Survey of Finland, unpublished report Q10.2/2009/61, 11–16.

Lokajíček, T., Pros, Z., Klíma, K., Nikitin, A. N., Ivankina, T. I., Ullemeyer, K., Smirnov, Y. P. & Kusnetzov Y. I. 2000. P-wave elastic anisotropy and texture of amphibolites from the Kola Super Deep Borehole KSDB-3. In: Mitrofanov, F. P. & Gorbatsevich, F. F. (eds.) The results of the study of the deep substance and physical processes in the Kola Superdeep Borehole section down to a depth of 12261 m.). Apatity: Poligraf Publishers, 122–125.

Orlov, V. P. & Laverov, N. P. (eds.) 1998. Kola Superdeep. Scientific results and research experience. Moscow: MF "Technoneftegas". 260 p. (in Russian)

Robin, P.-Y. F. 1979. Theory of metamorphic segregation and related processes. Geochimica & Cosmochimica Acta 43 (10), 1587–1600.

Volkova, E. A. 1974. Polarization measurements. Moscow: Publ. Standartov. 156 p. (in Russian)